AMERICAN SCIENTIFIC PUBLISHERS

Journal of Neuroscience and Neuroengineering
Vol. 2, pp. 1–12, 2014
(www.aspbs.com/jnsne)

RESEARCH ARTICLE

Overlapping Brain Activity as Reflected by the Spatial Differentiation of Functional Magnetic Resonance Imaging, Electroencephalography and Magnetoencephalography Data

Kuzma Strelnikov* and Pascal Barone

CNRS CERCO UMR 5549, Faculté de Médecine de Rangueil, Toulouse University, Pavillon Baudot CHU Purpan BP 25202, 31052 Toulouse Cedex, France

In classical neuroimaging, the activity of each voxel is considered separately. However, it was recently demonstrated that there are significant stimulation-specific differences between adjacent voxels at the group level. With this approach, the activity of adjacent voxels in the same condition is compared, and the direction of the highest increase of activity in the neighbourhood of each voxel is established as a gradient vector per voxel. Using this vector approach, we compared fMRI, EEG and MEG spatial differential activity during different tasks to see what amount of fMRI differential activity corresponds to the electromagnetic differential activity. Distributed source reconstruction was used to obtain 3-dimensional models of electric and magnetic activity in EEG and MEG prior to vector analysis. Using independent datasets, we illustrated that the mean overlap of the fMRI differential activity with EEG and MEG is 79%. In addition, about 93% of divergence (spatial sources) in fMRI corresponded to the EEG and MEG divergences. These results correspond to the spatial sum of the peak activities in EEG and MEG and, further, suggest a link between the spatial and temporal properties of brain activity. We propose a novel model of activity flows in the brain to explain this link.

KEYWORDS: fMRI, EEG, MEG, Vector Analysis, Spatial Differentiation, Activity Flows.

INTRODUCTION

To study brain function, various neuroimaging techniques measure the activity of neuroglial populations in the brain at rest and during stimulation. Due to neuropsychological traditions, classical neuroimaging primarily focuses on the existence of global activity in different brain areas. Mathematically, comparisons of activity in individual voxels for different types of stimulation are realized using various statistical techniques, from multi-level factor analysis to the simple *t*-test [1]. As a result, the classical approach to brain activity studies relies on the activity differences in the same voxel under different conditions.

Since the classical approach to brain activity studies does not address the differences between adjacent voxels constituting the internal structure of brain activity, we developed a new approach that compares activity in adjacent voxels under the same conditions. This computation provides the direction of the highest difference of activity in the neighbourhood of individual voxels. Thus, each voxel contains a vector pointing toward the direction of the highest activity difference in its neighbourhood, with the size of the vector reflecting the size of the increase (see Fig. 1). Using mathematical terms, we define the vector that is established per voxel as the gradient vector. In three dimensions, this method is mathematically similar to the current 2-dimensional source density analysis used in electrophysiology [2, 3]. Globally, this analysis results in maps of gradient vector projections that can be used to compare experimental conditions. We have demonstrated that spatial differences (gradients) of activity between voxels persist in different subjects, resulting in their significance at group level, even after family-wise error correction of *p*-values. We have shown that these gradients are task-specific [4]; therefore, they specifically reflect cognitive processes in the brain. Such an observation strongly suggests that gradient analysis is a promising alternative method for analysing brain function.

The proposed gradient maps provide novel information on the spatial organisation of brain activity. We hypothesized that the greatest spatial increase of activity may occur in the areas where there is a burst of activity in a

*Author to whom correspondence should be addressed.
Emails: kuzma@cerco.ups-tlse.fr, strelkuz@hotmail.com
Received: xx Xxxx xxxx
Accepted: xx Xxxx xxxx

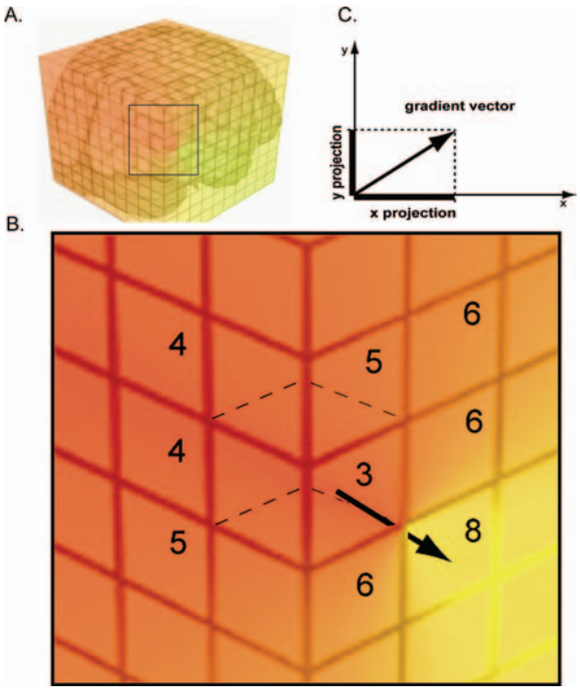

Fig. 1. Illustration of the gradient vector and its projections for the field of brain activity. (A) Functional neuroimaging represents the brain as a field of activity with a value per each small volume called voxel. (B) The gradient vector for each voxel points to the direction of the greatest increase. Here, for the voxel with energy level of 3 the greatest increase is in the direction of the voxel with the level of energy 8. The length of the vector represents the difference 8–3. (C) Each gradient vector can be considered in its projections on the axes. Here, the projections on the *X* and *Y* axes are illustrated (the projection on the *Z* axis is taken 0 and not shown).

specialized neural population and less activity in the input pathway. A high positive slope of activity increase at the places of functional inputs to specialized neural populations was demonstrated by some electrophysiological and computational studies [5, 6]. At the level of neuromediators, excitatory interpretations of these high positive slopes of activity increase are more probable because glutamate-related processes account for approximately 70% of total energy turnover [7], while GABAergic processes account for only about 15% of total energy turnover by neurons and glia [8]. Thus, the greatest activity increase would be at the locus receiving the informational input, which anatomically corresponds to the input from the long- or short-range connections [9]. Based on this interpretation, differential analysis, being local by nature, does not consider long-range connections in the brain along their whole length. These connections are detectable only at their target points, when they cause an abrupt increase of activity in the specialized population. One can search for long-range connections using these target points as seed points for connectivity analysis [10] at the functional level and for diffusion tensor imaging [11, 12] at the anatomical level. The gradient indicates the direction of the abrupt increase in activity, which, in turn, may correspond to the direction of the signal input to a specialised population. If the abrupt activity increase occurs each time after the presentation of a stimulus, one can detect the input direction in the time-averaged image of brain activity.

Though the above hypothesis seems plausible, the exact physiological interpretation of the experimentally observed gradients of activity requires further study to define the neural support of such gradients. One strategy to assess the physiology of gradients would be to compare them between different modalities of brain activity (Functional Magnetic Resonance Imaging (fMRI), Electroencephalography (EEG) and Magnetoencephalography (MEG)), because the substrates are more or less understood. Though the nature of the Blood-Oxygen-Level-Dependent (BOLD) signal is not entirely understood, it may reflect the input and intracortical processing of a given area rather than its spiking output [13]. Similarly, it is believed that the postsynaptic potentials of large cortical pyramidal neurons in deep cortical layers play a major role in the generation of the EEG [14] and MEG [15].

The fMRI measurement of brain activity is not direct but is a complex function of oxygen consumption and regional blood flow [16, 17]. In spite of this complexity of the BOLD signal, what makes us confident in our approach is the demonstrated proportionality between the BOLD signal and human EEG measurements [18, 19]. Besides, the approximate proportionality between the BOLD signal and electrical activity, which corresponds to the proportionality between metabolic and electric energies, was tested locally in neural populations [20, 21].

These considerations of the nature of the BOLD and EEG signals with respect to cortical inputs suggest a rather high spatial overlap between these techniques when one calculates spatial gradients, which, according to our hypothesis, emphasizes the directions of cortical inputs. Given that some dissociations of the BOLD signal and electrophysiological data are also reported [22], one cannot expect 100% overlap, but an overlap greater than 50% can be interpreted as a reasonable result corresponding to the variable literature data on fMRI-electrophysiological coupling.

The purpose of this study is to determine whether the spatial distribution of the gradient vectors derived from fMRI activity corresponds to the spatial distribution of the gradient vectors obtained from electric and magnetic activities. For the whole brain, we expect that the differences between the neighbouring voxels, as found by the analysis of gradient vectors, will have similar spatial distribution among different neuroimaging techniques.

In consequence, in this study we compute fMRI, EEG and MEG gradient activity maps and spatially compare them to estimate whether the spatial distribution of gradients in fMRI activity corresponds to the spatial distribution of gradients in EEG and MEG, calculated on the basis of distributed source reconstruction.

EXPERIMENTAL DETAILS

In this article, we use an exemplary dataset available on the site of statistical parametric mapping (SPM), which is commonly used to elaborate comparative methods in neuroimaging [23–26]. This dataset contains EEG, MEG, functional MRI and structural MRI data on the same subject with the same paradigm: a basic comparison of faces versus scrambled faces. The task was left–right symmetry judgement [27]. Famous and non-famous (unfamiliar) greyscale faces (52 of each) were presented. These faces were split into two sets of 26 famous (familiar) and 26 non-famous (unfamiliar) faces (8 female faces and 16 male faces in each set). The faces were presented for 500 ms, replacing a baseline of an oval chequerboard present throughout the interstimulus interval, with a stochastic distribution of stimulus onset asynchrony (SOA) determined by a minimal SOA of 4.5 s and 52 randomly intermixed null events. Each stimulus was presented on a mirror 30 cm above the participant, subtending a visual angle of $\sim 10°$.

For the fMRI data acquisition, the 2-T VISION system (Siemens, Erlangen, Germany) was used to acquire 32 T_2^*–weighted transverse echoplanar images (EPI) (64×64 3×3 mm^2 pixels, $T_E = 40$ ms) per volume, with blood oxygenation level dependent (BOLD) contrast. EPIs comprised 2 mm thick axial slices taken every 3.5 mm, acquired sequentially in a descending direction. The EEG data with the same stimulation and task were acquired on a 128-channel ActiveTwo system; the MEG data were acquired on a 275-channel CTF/VSM system.

All data were analyzed with SPM8 following the recommendations of the SPM8 manual for this dataset.

As a supplementary analysis, we used the fMRI-MEG data during auditory perception from the study of Babajani-Feremi et al. [28], subject 07 (please see the original publication for the details of the experimental paradigm and acquisition). An analysis similar to that for the main dataset was applied.

In addition, we decided to include the application of this analysis to the dataset of the simultaneous fMRI-EEG pilot study from our laboratory. Although the simultaneous fMRI-EEG has some technical problems [29], this approach is gaining popularity [30] and could be of interest to readers. In this pilot study, a white circle was presented in the left superior visual quadrant for 6 ms on a black screen, eccentricity 2.5°, 3.5° in diameter, with a random SOA of 2–14 s. A Brain Products 64-electrode EEG cap specially designed for the fMRI studies was used. In the 3T Philips fMRI scanner, functional scans were acquired with a single-shot echo planar gradient-echo (EPI) pulse sequence (TR = 2 s, TP = 30 ms, flip angle = 77°, FOV = 215 mm, matrix = 64×64). An FMRIB Plug-in for EEGLAB was used to remove the fMRI artefacts from the EEG, including the pulse/ballistocardiographic artefacts [31]. It was a passive perception paradigm.

fMRI Data Analysis

The time-series for each voxel was highpass-filtered to 1/128 Hz and realigned temporally to acquisition of the middle slice. The highpass-filter of 1/128 Hz is provided by default in the SPM analysis, and we checked that most of the experimental variance was not removed by this filter. No other method of physiological noise reduction was used. Given that the main multimodal dataset used here is available on the site of SPM, we followed exactly the pipeline of analysis for this dataset proposed in the SPM8 manual so that it could be easily reproduced.

Images were normalized to a standard EPI template based in Talairach space and resampled to $3 \times 3 \times 3$ mm^3 voxels. The normalized images were smoothed with an isotropic 8 mm full-width-at-half-maximum (FWHM) Gaussian kernel (final estimated smoothness was $10 \times 10 \times 10$ mm^3 FWHM). No smoothing was applied to the spatially differentiated images of the fMRI activities. The implicit SPM mask was applied to all fMRI images.

Gradient and divergence calculations were applied [4] to the pre-processed fMRI images, leading to the creation of four images for each pre-processed image: X gradient image (projection of the gradient vector on the X axis), Y gradient image, Z gradient image and divergence image. Separate gradient images for each projection as well as divergence images were entered into the first-level analysis with the canonical HRF and time and dispersion derivatives. Thus, four model matrices were constructed. The t-contrasts 'faces versus scrambled faces' and 'scrambled faces versus faces' were defined, resulting in two corresponding contrast images for each model matrix. The contrast images were thresholded at $p < 0.001$ uncorrected level (in the supplementary datasets, also adjusted to maximize the overlap) and used for further comparative analyses with EEG and MEG data. Thus, we used the whole fMRI time-series and normalized the stimulation-related activity to the baseline activity.

Numerical gradients with finite difference approximation are used as implemented in the MATLAB gradient function. For example, for the x dimension FX = gradient (F, x); $\mathrm{FX}(i) = (F(i+1) - F(i-1))/(x(i+1) - (i-1))$, the first and last points are first order approximations: one is a forward difference and the other is a backward difference; the points inside the row are second order approximations.

EEG and MEG Data Analysis

Epochs were defined as a peri-stimulus time window that started at -200 ms and ended at 600 ms. Artefact rejection was done by rejecting trials in which the signal recorded at any of the channels exceeded 200 microvolts relative to the pre-stimulus baseline.

3D reconstruction was performed by the method of distributed source reconstruction using a gray-matter mesh extracted from the subject's MRI and the Multiple Sparse Priors (MSP) [25, 32]. This method corresponds to a

distributed source localisation, where current sources are estimated at a large number of fixed points within a cortical mesh. Thus, this method permitted overlaying the measurements of electromagnetic fields on the scalp with the distribution of this field in the 3D brain space, making the resulting images comparable with the 3D data obtained by fMRI. In EEG data, we calculated for each voxel the mean amplitude of the distributed source activity during the periods of 170–190 ms and 360–380 ms, which corresponded to the periods of peak activity. In MEG data, mean amplitudes were also calculated during the periods of 170–190 ms and 360–380 ms, and in addition, a third time point of 380–400 ms was calculated because at some locations it was separate from the peak at 360–380 ms. The 3D datasets with peak amplitude per voxel were transformed into images of gradient projections on the X, Y and Z axes, plus a divergence image for each peak. Thus, images of gradient projections and divergence images were obtained for the time points of the source activity in EEG and MEG. The initial M/EEG images were smoothed with an isotropic 12 mm FWHM Gaussian kernel. No smoothing was applied to the spatially differentiated images of the M/EEG activities.

Comparison of fMRI, EEG and MEG Data

First, we created 3D images of distributed sources in EEG and MEG with mean values in the chosen time windows at the peaks of activity. Then, gradients and divergence were calculated in these images. To create the masks of positive gradient projections, positive values were replaced with ones and all other values with zeros. To create the masks of negative gradient projections, negative values were replaced with ones and all other values with zeros. Then fMRI images of positive and negative gradient projections were multiplied element by element by the corresponding mask images.

To calculate the number of active voxels in the non-masked fMRI images, fMRI images of positive and negative gradient projections were transformed into ones and summed up. In the same way, the masked fMRI images were transformed into ones and summed up. This permitted us to separately calculate the relation between the number of active voxels in the masked and non-masked fMRI images for each peak.

As we were interested in the spatial overlap among different peaks in EEG and MEG inside the fMRI areas, we multiplied element by element the masked fMRI images corresponding to different peaks and transformed the results into ones (separately for EEG and MEG). The sum of the surviving voxels provided the number of voxels in the spatial overlap.

To obtain the number of voxels in the fMRI differential activity corresponding to electromagnetic differential activity, we first calculated a spatial sum of the masked fMRI images transformed into ones corresponding to the peaks in the EEG and MEG data. As a result, some of the voxels had a value of 2; to eliminate this we again replaced the positive numbers in the images with ones. In this way, we could avoid calculating the areas of spatial overlap twice. Finally, the sum of these images was calculated, which provided the number of voxels within the differential fMRI activity corresponding to the spatial sum of peaks in EEG and MEG data. The relation of this sum to the sum of voxels in the non-masked fMRI images was calculated, which provided the percent of fMRI activity corresponding to the summary EEG and MEG activities.

Projections Used in the Analysis

As we have recently shown [4], brain activity can be characterized by the different directions of gradient vectors. For practical purposes, it is useful to consider the significant projections of these vectors on the three principal axes in the MNI or Talairach conventions of brain coordinates. In these conventions, the X axis goes from left to right, the Y axis goes from back to front and the Z axis goes upwards. If projections on an axis in a given region are positive, it implies that the direction of most gradient vectors in this region corresponds to the direction of the axis. If projections are negative, it follows that gradient vectors in this region are mostly in the opposite direction. E.g., when there are positive projections on the X axis in some clusters, one can conclude that in these clusters the more rapid changes of the BOLD signal are in the positive direction of the X axis (the 'left-right' direction). According to our hypothesis of energy flows [4], the predominant direction of energy flows in these clusters is from left to right.

Positive divergence is observed in the regions where the summary flow of gradient vectors from the voxels is outside. We suggested that these voxels may constitute a source of energy flows for the neuroglial population in adjacent voxels [4].

Explanatory Model of Energy Coupling and Energy Flows

Given the average metabolic energy M and electromagnetic energy E corresponding to each time period from 1 to n, the result can be presented this way (the sign ∇ means gradient):

$$\nabla M = k_1 \nabla E_1 + k_2 \nabla E_2 + k_3 \nabla E_3 + k_n \nabla E_n \qquad (1)$$

Here, M as well as indexed E and coefficients k are the functions of position (with the coordinates x, y, z). This equation presents a relation between the spatial distribution of M and the temporal changes in E in the time periods from 1 to n. As gradients are vectors, the equation can be rewritten in terms of vector projections on the axes, e.g., for an axis x it would be:

$$\nabla M_x = k_{x1} \nabla E_{x1} + k_{x2} \nabla E_{x2} + k_{x3} \nabla E_{x3} + k_{xn} \nabla E_{xn} \qquad (2)$$

where again M_x as well as indexed E_x and coefficients k_x are the functions of position (x, y, z).

The three projections can be explicitly expressed in the matrix form:

$$\begin{bmatrix} \nabla M_x \\ \nabla M_y \\ \nabla M_z \end{bmatrix} = \begin{bmatrix} \nabla E_{x1} \dots \nabla E_{xn} \\ \nabla E_{y1} \dots \nabla E_{yn} \\ \nabla E_{z1} \dots \nabla E_{zn} \end{bmatrix} \cdot \begin{bmatrix} k_{x1} & k_{y1} & k_{z1} \\ \dots & & \\ k_{xn} & k_{yn} & k_{zn} \end{bmatrix} \quad (3)$$

This formula corresponds to the practical calculations we used in this study, but we can try to rewrite it in a more general form. One can express the electromagnetic energy E_n at each time period as a product of the rate of its change during this period v_n and the time period Δt. Always taking the same time period and omitting for simplicity the coefficients k, we get:

$$\nabla M \propto \nabla v_1 \Delta t + \dots \nabla v_n \Delta t = \nabla (v_1 + \dots v_n) \Delta t = \nabla \sum_{i=1}^{i=n} v_i \Delta t \quad (4)$$

Supposing very small time periods δt, we pass from the sum to the integral over the whole time of measurement from time t_1 to time t_2:

$$\nabla M(x, y, z) \propto \nabla \int_{t_1}^{t_2} v(x, y, z, t) \delta t \quad (5)$$

Or in the form of projections on the axes and including the coefficients p:

$$\begin{bmatrix} \nabla M_x \\ \nabla M_y \\ \nabla M_z \end{bmatrix} = \nabla \int_{t_1}^{t_2} \begin{bmatrix} p_x v_x \\ p_y v_y \\ p_z v_z \end{bmatrix} \delta t \quad (6)$$

Here, indexed v and p are the functions of (x, y, z, t). This general formula presents the relationship between the gradients of the average metabolic energy from time t_1 to time t_2 and the gradients of electromagnetic energy in this period. It can be further clarified by a simple consideration. The average metabolic energy can also be presented as a sum of the products of its rate of change m over a small period of time Δt, and the whole sum then divided by the number n of such periods of time:

$$M(x, y, z) = \frac{1}{n} \sum_{i=1}^{i=n} m_i \Delta t \quad (7)$$

Presenting it in the limit of very small time periods δt as the integral

$$M(x, y, z) = \frac{1}{t_2 - t_1} \int_{t_1}^{t_2} m(x, y, z, t) \delta t \quad (8)$$

we obtain from (5)

$$\nabla \frac{1}{t_2 - t_1} \int_{t_1}^{t_2} m(x, y, z, t) \delta t \propto \nabla \int_{t_1}^{t_2} v(x, y, z, t) \delta t \quad (9)$$

leaving only the expressions under the integral

$$m(x, y, z, t) \propto v(x, y, z, t) \quad (10)$$

It should be noted that metabolic measurement here is a measurement of metabolic energy at each time point, which is potentially possible in future techniques but is not possible for the BOLD technique at present. The approximate proportionality is demonstrated by several experiments [20, 21]; it can be considered as indirect evidence for Eq. (6), complementary to the direct evidence from our results, on which Eq. (6) is based. Correlations between the BOLD and electric activity varied between the studies in a range from 0.7 [13] up to 0.9 [18, 19], depending on the technique used. Thus, the proportionality is only a linear approximation of more complex processes, which is why in our explanatory Eq. (6) we have a set of unknown parameters in the form of coefficients p, which adjust the equation for each time point. Generative models aim to provide exact parameters; as a result, relationships between the electric, metabolic activity and the fMRI signal in these models are much more complex [33]. On the other hand, the spatial correspondence shown here between the vectorial representations of brain activity in different modalities could be further implemented in the generative models to increase their precision.

It should also be noted that we considered only the changes of metabolic energy coupled with information processing. In general, part of metabolic energy is also used for cellular maintenance unrelated to information processing and part is dissipated as heat.

Let us consider the sum (ΔS) of information-related metabolic (ΔM) and electromagnetic (ΔE) energy increases in a voxel at a given moment of time (the sign Δ for the difference here should not be confused with the gradient sign ∇):

$$\Delta S = \Delta M + \Delta E \quad (11)$$

as ΔM is approximately proportional to ΔE and metabolic energy is transformed into electromagnetic. We can also write this as:

$$\Delta S = k \Delta E + \Delta E \quad (12)$$

where $\mathbf{k}$ is a certain proportionality coefficient between information-related metabolic and electromagnetic energies. Essentially, $\mathbf{k}$ shows how much electromagnetic energy is added to this voxel due to the amplifying input of metabolic energy. Let us consider three neighbouring voxels along the X axis (Fig. 5). The first two voxels serve only to propagate information to the third voxel, where this information is treated. Signal propagation is realized by electromagnetic fields. Each time the electromagnetic signal ΔE arrives at these voxels, the summary energy increase ΔS_1 and ΔS_2 in each voxel is approximately ΔE; metabolic energy amplifies the electromagnetic signal very little and the coefficient $\mathbf{k}$ is small. However, when the information-related energy increase ΔE arrives at the third voxel, this increase used for propagation becomes insufficient for information treatment. A high input of

metabolic energy is required, and is further transformed into additional electromagnetic energy. Thus, the coefficient **k** becomes high, leading to a significant increase in ΔS_3 in the third voxel. The gradient (energy increase) along the X axis between the first two voxels is $\mathrm{Gr}_{1-2} = \Delta S_2 - \Delta S_1$ and between the second and the third voxel is $\mathrm{Gr}_{2-3} = \Delta S_3 - \Delta S_2$. Evidently,

$$\mathrm{Gr}_{2-3} > \mathrm{Gr}_{1-2} \tag{13}$$

As in our analysis, the gradient is indicated for each voxel. In this one-dimensional situation the second voxel would contain a value Gr_{2-3}. The positive value indicates that the increase direction from this voxel corresponds to the positive direction of the X-axis. From Eq. (5), the average difference in metabolic energy between the third and the second voxels will be related to the time course of the electromagnetic energy difference:

$$\nabla M(x) \propto \nabla \int_{t_1}^{t_2} v(x,t)\delta t \tag{14}$$

Thus, one can see that stable energy gradients between voxels correspond to the direction of electromagnetic energy flows to the specialized neuroglial populations [34]. Metabolic energy is transformed into electromagnetic energy, amplifying it in the specialized neuroglial population (voxel 3 in Fig. 5). Our model is not specific to the BOLD signal; it aims to explain the brain phenomena behind the measurement techniques, and we suggest that it can be applied to any measurement that reflects metabolic energy turnover in the brain (e.g., PET measurements and other techniques of brain metabolism measurements possible in future studies [35]).

RESULTS

The classical analysis of fMRI, EEG and MEG activities during the face processing task reproduced the same pattern of activity as in previous studies of this dataset with maximal activity in the occipital, inferior temporal and frontal regions (see SPM8 manual, 'Multimodal face-evoked responses' [36]).

The summary whole-brain overlap in the original activation data was 47% between fMRI and EEG and 34% between fMRI and MEG. Strelnikov and Barone [4] have shown that activation maps and maps of differential activity are totally different. Differential activity is not detected within the areas of classical activity because absolute values and differential values represent independent datasets.

We then proceeded with analysis of the spatial differentiation data in order to quantitatively compare its results among different techniques. First, we compared the spatial differential brain activity in fMRI and in EEG distributed source reconstruction spatial maps. The comparison was performed with respect to the activity observed in fMRI for the projections of the gradient vector on the X, Y and Z axes according to the MNI coordinate system separately for the positive and negative directions of each axis. For both the positive and negative directions, the significant gradient vector projections in the fMRI activity were detected in the occipital and inferior temporal regions bilaterally (Figs. 2, 3).

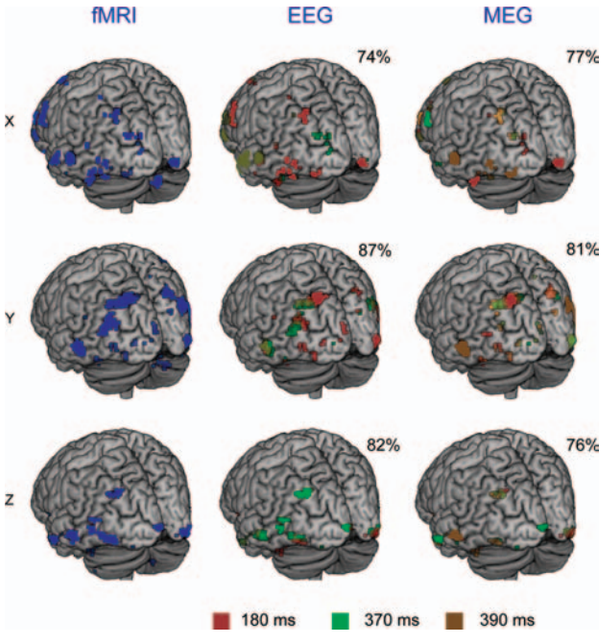

Fig. 2. Positive directions of the fMRI differential activity corresponding to EEG and MEG. The left column represents the negative projections of the gradient vectors in the fMRI activity on the X, Y and Z axes in the MNI space. Time points of 180 ms, 370 ms and 390 ms, around which EEG and MEG data was sampled, are presented in colours (the spatial overlap in some regions modifies the initial colours). The percent indicates the spatial sum of these time points, taking into account their spatial overlap.

For the positive directions of X, Y and Z, the EEG activity overlapped, respectively, at 74%, 87% and 82% with the fMRI activity, taking into account the overlaps among the peaks (Table I, Fig. 2). As for the negative projections on these axes, the respective values are 91%, 89% and 93% (Table I, Fig. 3).

Concerning the divergence (spatial sources) of gradient vectors (Table III, Fig. 4), the spatial distribution of the first EEG peak corresponded to 70% and of the second to 38% of the divergence in fMRI. With an overlap of 17%, the overlap of divergence with fMRI was 95%.

Thus, depending on the direction of the gradient projection, 74–93% of the fMRI differential activity overlapped with the EEG differential activity. The percent of the EEG divergence overlapping with fMRI was even higher at 95%.

Next, we compared the spatial differential brain activity in fMRI and in MEG distributed source reconstruction spatial maps in a similar manner. This comparison was also performed separately for the positive and negative directions of each axis with respect to the activity observed in

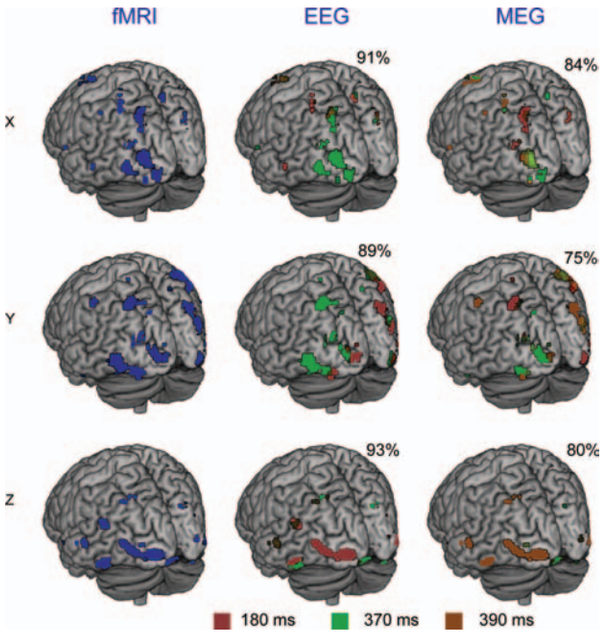

Fig. 3. Negative directions of the fMRI differential activity corresponding to EEG and MEG. The left column represents the negative projections of the gradient vectors in the fMRI activity on the *X*, *Y* and *Z* axes in the MNI space. Time points of 180 ms, 370 ms and 390 ms, around which EEG and MEG data was sampled, are presented in colours. The percent indicates the spatial sum of these time points taking into account their spatial overlap.

fMRI for the projections of the gradient vector on the *X*, *Y* and *Z* axes according to the MNI coordinate system. The main difference for the EEG is that due to the variability of the peak corresponding to the second peak in the EEG, the third peak was also included in the analysis.

Thus, regarding the positive directions of axes *X*, *Y* and *Z*, the MEG activity overlapped at 77%, 81% and 76% respectively with the fMRI activity, taking into account the overlaps among the three peaks (Table II, Fig. 2). As for the negative projections on these axes, the

Table I. Percent of the fMRI differential activity corresponding to the EEG differential activity.

	Peak 1 (%)	Peak 2 (%)	Overlap (%)	Total (%)
		Positive directions		
X	48	40	28	74
Y	42	53	21	87
Z	48	52	36	82
		Negative directions		
X	39	72	50	91
Y	59	42	21	89
Z	57	57	35	93

Notes: *X*, *Y*, *Z* indicate the images of the projections of the gradient vector on the axes, in positive and negative directions. Peak 1 of EEG activity corresponds to 170–190 ms and Peak 2 to 360–380 ms. Overlap is indicated with respect to the fMRI activity corresponding to peak 1. Total is the spatial sum of Peak 1 and Peak 2 where regions of their overlap are calculated only once.

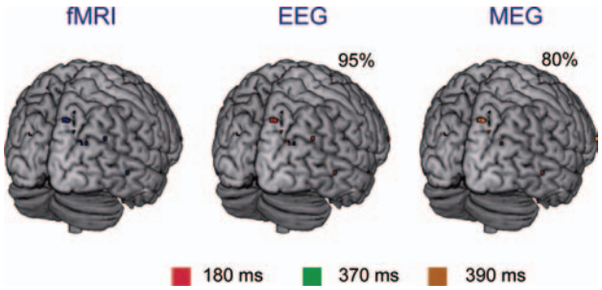

Fig. 4. Divergences of the fMRI differential activity corresponding to the EEG and MEG differential activity divergences. Time points of 180 ms, 370 ms and 390 ms, around which EEG and MEG data was sampled, are presented in colours. The percent indicates the spatial sum of these time points taking into account their spatial overlap.

corresponding values were 84%, 75% and 80% (Table II, Fig. 3).

Considering the divergence (spatial sources) of gradient vectors for MEG and fMRI (Table III, Fig. 4), 62%, 39% and 52% of the fMRI divergence overlapped with the first, the second and the third MEG peaks respectively. Taking into account the overlaps of 46–65% between peaks, the MEG divergence corresponded to 80% of the fMRI divergence.

Thus, depending on the direction of the gradient projection, 75–84% of the fMRI differential activity overlapped with the MEG differential activity. The overlap of the divergence between fMRI and MEG was 80%.

As both positive and negative deviations in EEG and MEG reflect an increase of neural activity, we tried other methods of calculation, inversing the signs and taking the absolute values of the EEG and MEG distributed source reconstruction spatial maps. Both of these methods turned out to be less efficient in explaining the differential fMRI activity, the summary explanatory percent being only about 40–50. For instance, if there are two neighbouring voxels with activity levels of −5 and 7, the original analysis gives the gradient value of 12, the absolute values analysis gives the gradient value between 5 and 7, a difference of only 2, and the inversed sign analysis gives the gradient value between 5 and −7, which has the same value of 12, but the gradient vector points to the voxel 5 instead of the voxel 7 in the original analysis. Thus, the absolute value analysis decreased the correspondence with fMRI by the decreased gradient values, and the inversed sign analysis decreased the spatial correspondence with fMRI gradients.

In the supplementary analysis of the fMRI-MEG auditory dataset, the overlap between gradient projections was 56–100% (mean 80%) with 96% overlap for the divergence (Table IV). In the simultaneous EEG-fMRI dataset, the overlap between gradient projections was 51–100% (mean 72%) and 100% for the divergence (Table V).

If one considers all the fMRI-M/EEG comparisons in the datasets of this study, the mean overlap for the gradient projections for EEG is $79 \pm 10\%$ ($p < 0.05$, bootstrap bias

Table II. Percent of the fMRI differential activity corresponding to the MEG differential activity.

	Peak 1 (%)	Peak 2 (%)	Peak 3 (%)	Overlap 1–2 (%)	Overlap 2–3 (%)	Overlap 1–3 (%)	Total (%)
				Positive directions			
X	55	50	47	65	53	66	77
Y	48	61	62	66	83	76	81
Z	40	45	40	33	55	57	76
				Negative directions			
X	47	45	59	46	70	60	84
Y	53	32	42	28	69	48	75
Z	49	53	53	50	74	67	80

Notes: *X*, *Y*, *Z* indicate the images of the projections of the gradient vector on the axes, in positive and negative directions. Peak 1 of MEG activity corresponds to 170–190 ms, Peak 2 to 360–380 ms and Peak 3 to 380–400 ms. Overlap is indicated with respect to the fMRI activity corresponding to the earlier peak. Total is the spatial sum of Peak 1, Peak 2 and Peak 3 where regions of their overlap are calculated only once.

Table III. Percent of the divergences in fMRI corresponding to the EEG and MEG divergences.

Divergence	Peak 1 (%)	Peak 2 (%)	Peak 3 (%)	Overlap 1–2 (%)	Overlap 2–3 (%)	Overlap 1–3 (%)	Total (%)
EEG	70	38		17			95
MEG	62	39	52	46	65	63	80

Note: Peak 1 of MEG activity corresponds to 170–190 ms, Peak 2 to 360–380 ms and Peak 3 to 380–400 ms. Overlap is indicated with respect to the fMRI activity corresponding to the earlier peak. Total is the spatial sum of Peak 1, Peak 2 and Peak 3 where regions of their overlap are calculated only once.

corrected and accelerated confidence intervals [37]) and for MEG, $79 \pm 7\%$ ($p < 0.05$). The mean overlap for the divergences in the EEG and MEG datasets is $93 \pm 7\%$ ($p < 0.05$).

DISCUSSION

In this study, we compared the fMRI, EEG, and MEG spatial differential activity during an identical task of face processing. After the conventional fMRI analysis, distributed source reconstruction [32] was used to obtain the 3-dimensional models of electric and magnetic activity in EEG and MEG. Then we performed a gradient vector calculation for the spatial maps of fMRI, EEG, and MEG. Decomposing the gradient vector into its projections on the *X*, *Y*, and *Z* axes, we estimated, for each axis, the percentage of fMRI data corresponding to the spatial sum of the sampled activities in EEG and MEG.

Our results suggest a close link between the spatial differential activity (spatial gradients) measured using different neuroimaging techniques. For the main dataset, we showed that 74–93% of the fMRI differential activity overlaps with EEG and 75–84% overlaps with MEG differential activity. In addition, 95% of divergences (spatial sources of gradient vectors) in fMRI overlap with the EEG divergences and 80% overlap with the MEG divergences. High overlaps were also detected in the supplementary datasets with different stimulation paradigms. If one considers all the fMRI-M/EEG comparisons, including the supplementary datasets of this study, the mean overlap for the gradient projections for EEG is $79 \pm 10\%$ ($p < 0.05$) and for MEG, $79 \pm 7\%$ ($p < 0.05$). The mean overlap for the divergences in the EEG and MEG datasets is $93 \pm 7\%$ ($p < 0.05$).

The high overlap between different modalities is in line with the idea that, for different measurements of brain

Table IV. Percent of the fMRI differential activity corresponding to the MEG differential activity in the auditory dataset.

	Peak 1 (%)	Peak 2 (%)	Peak 3 (%)	Overlap 1–2 (%)	Overlap 2–3 (%)	Overlap 1–3 (%)	Total (%)
				Positive directions			
X	61	61	100	100	100	100	100
Y	28	68	79	100	100	100	79
Z	60	62	81	99	94	96	85
				Negative directions			
X	44	55	44	100	80	100	56
Y	53	51	58	98	97	95	60
Z	100	100	100	100	100	100	100
				Divergence			
	47	32	39	68	93	77	96

Note: Total is the spatial sum of Peak 1, Peak 2 and Peak 3 where regions of their overlap are calculated only once.

Table V. Percent of the fMRI differential activity corresponding to the EEG differential activity in the simultaneous fMRI-EEG dataset.

	Peak 1 (%)	Peak 2 (%)	Peak 3 (%)	Overlap 1–2 (%)	Overlap 2–3 (%)	Overlap 1–3 (%)	Total (%)
				Positive directions			
X	33	6	56	17	100	100	56
Y	66	25	54	78	100	81	67
Z	55	53	53	93	96	94	57
				Negative directions			
X	100	100	100	100	100	100	100
Y	46	52	51	100	100	100	51
Z	100	100	100	100	100	100	100
				Divergence			
	100	100	92	100	92	92	100

Note: Total is the spatial sum of Peak 1, Peak 2 and Peak 3 where regions of their overlap are calculated only once.

activity, the greatest activity difference in space should be at the loci receiving the informational input, which anatomically corresponds to the input from the long- or short-range connections [9]. The high spatial increase of activity in these regions stems from the fact that there is a small amount of activity in neural pathways compared with the activity in specialized neuroglial populations where the pathways terminate [5, 6]. Besides, this corresponds to the evidence that the BOLD signal mostly reflects the inputs to the neural populations of the cortex [13] and that the EEG signal reflects the post-synaptic potentials of the cortical neurons [14]. Thus, the novel method of spatial differentiation (spatial gradients) reveals the task-related distribution of information inputs to the cortex on the basis of the complex network of anatomical pathways within the brain. Compared with classical activations, this method provides a complementary view of the functional organisation of brain activity, emphasizing the task-related changes of activity propagation along the pathways at their arrival loci in the specialized neuroglial populations. As these results correspond to the spatial sum of the peak activities in EEG and MEG, they suggest a novel link between the spatial and temporal properties of brain activity in light of the local differences of activity between the neighbouring voxels.

Relationship Between the Fields of Metabolic and Electromagnetic Activities

Along with methodological issues, the fundamental issue we consider in this article is whether the spatial distribution of the gradient vectors of fMRI activity corresponds to the spatial distribution of the gradient vectors of electric and magnetic activities. Our results suggest that the gradient of the mean BOLD signal can be expressed as the spatial sum of the gradients of electric and magnetic fields at different points in time. The BOLD signal reflects the metabolic demands of the brain, thereby enabling the measurement of metabolic energy.

Our results suggest that the spatial distribution of gradients in the fMRI activity may significantly overlap the EEG and the MEG differential activity. In our previous study [4], when comparing the results of the activation analysis with the results for the spatial differentiation (gradient) analysis, we showed that the latter provided additional information about brain activity. The results of this study confirm the potential importance of the proposed method to clarify details about the distribution and dynamics of brain response and, in particular, about the directions of information-related activity distribution in the brain. Also, a potentially important output of this analysis is the localization of the sites in the brain cortex with a significant divergence of gradient vectors. According to the aforementioned conception of activity inputs, there is a net outflow of activity in these sites to the neighboring brain structures.

Since EEG and MEG peaks can be considered to be the temporal property of brain activity, their close link with the average fMRI activity in our study confirms a link between the temporal and spatial properties of brain activity. The spatial differential analysis for each peak in M/EEG indicates the gradient for each voxel at this point in time. When considering the activity gradients as reflectors of activity input paths in the brain, one can say that the temporal distributions of activity inputs observed in EEG form the average path of activity input as indicated by the vector analysis of fMRI activity.

As can be seen in Tables I and II of the main dataset analysis, as well as in Tables IV and V of the supplementary datasets analyses, the gradients of the M/EEG activity for each peak are combined to form the gradients of fMRI activity. Each volume within the fMRI activity corresponds either to the overlap between different M/EEG peaks (which can be from 21% to 100% according to our data) or only to one peak in M/EEG. This presence or absence of overlap between the gradient projections of the peaks within the fMRI gradient projections can also be clearly observed in Figures 2 and 3. One could suggest that gradients of fMRI activity per small volume correspond to the sum of gradients in the M/EEG activity, with a specific weight for the gradient of each peak. We believe that this relationship is not specific to fMRI but should be true for any measurement of brain metabolic

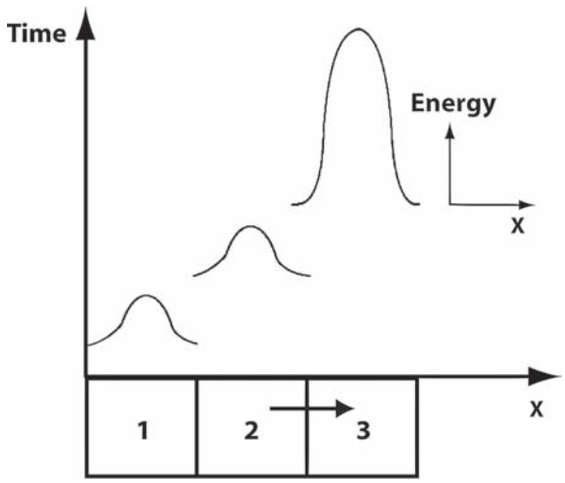

Fig. 5. A one-dimensional model of activity propagation in a given direction. Three voxels are presented along the horizontal *X* axis. Voxels 1 and 2 serve to transmit the signal to the specialized neuroglial population in voxel 3. The vertical time axis shows that the small increase of energy in voxel 1 is followed by the small increase of energy in voxel 2, followed by the large increase of energy in voxel 3. In voxel 3, the increase of electromagnetic energy received as a signal from voxel 2 is amplified using metabolic energy. The arrow pointing from voxel 2 corresponds to the gradient vector calculated in the present analysis, which indicates the direction of the greatest energy increase in the neighbourhood of voxel 2.

activity (e.g., with PET), and we propose a 1-dimensional model of activity propagation in the brain (see Fig. 5 and Section 2.5 of Experimental details) to help explain the link between electromagnetic and metabolic energy for any direction in the brain. In this model of activity propagation, metabolic energy is transformed into electromagnetic energy, amplifying it in the specialized neuroglial population. From this model, it is evident that metabolic energy gradients between voxels correspond to the direction of electromagnetic inputs to the specialized neuroglial populations [34].

Fusion of the fMRI, EEG, and MEG Data

M/EEG and fMRI fusion for the classical non-differentiated activity presents an expanding field of methodological and theoretical research; however, this fusion is complex because each method is only an approximate measure of neuronal activity. While M/EEG has high temporal but low spatial precision, fMRI has higher spatial precision based on the complex relationship between metabolism, oxygenation and blood flow, but provides temporally smoothed correlates of neuronal activity. To place our study in the context of the M/EEG and fMRI fusion studies, one should note that M/EEG–fMRI fusion approaches can be classified as [38]:

(1) asymmetric EEG to fMRI approaches,
(2) asymmetric fMRI to M/EEG approaches and
(3) symmetric fusion approaches.

M/EEG to fMRI approaches aim to benefit from the high temporal resolution of M/EEG, while fMRI to M/EEG approaches exploit the higher spatial precision of fMRI. Because we are interested in the spatial distribution of time-averaged gradients, our approach can be classified as an fMRI to M/EEG approach. Symmetric fusion approaches use generative models of neuronal activity to simulate both fMRI and M/EEG signals (e.g., on the basis of post-synaptic activity modelling [28], the number of active synapses per voxel [33] and the mechanisms of oscillatory activity [39, 40]). These generative models of neuronal activity present an opportunity for further elaboration of the spatial differentiation approach described herein.

The discrepancy between the EEG and MEG waveforms observed in this study already exists in the classical analysis (see the SPM8 manual). Our spatial differential analysis also revealed differences between EEG and MEG with respect to the fMRI clusters. The most striking difference can be observed in Figure 3 for the *Z*-axis negative projections: the occipital cluster in fMRI corresponds to the early peak in EEG and to the late peak in MEG. On the other hand, for the occipital cluster of the *Y* projections in the same figure, both the EEG and MEG data include the same peaks at 180 ms. The comparison between EEG and MEG is not related to the question of this study; however, it is noteworthy that the observed difference in time course and spatial distribution between EEG and MEG is not due to the spatially uncoupled electric and magnetic fields, which is physically impossible, but is due to the technical constraints of the techniques: while EEG has cortical generators in the superficial layers of the cortex (dipoles, mostly radial to the scalp surface), MEG cortical generators are in the vertical walls of the cortical sulci (dipoles tangential to the scalp surface) [41]. Besides, there are other potentially important differences in the nature of the MEG and EEG signals (see [15] for discussion of MEG). For example, the magnetic permeability of tissues is practically the same as that of empty space, thus the MEG signal is not distorted as it passes through tissue layers inside and outside the brain. On the contrary, the EEG signal on the scalp is distorted by many layers of various tissues (white matter, gray matter, meninges, cerebrospinal fluid) because they have different degrees of resistance.

Methodological Peculiarities of This Study

Several methodological constraints, which are important for the interpretation of these results, concern spatial reconstruction, contrasting with the baseline, source analysis, and temporal averaging of activity.

The spatial comparison in 3-dimensional space presents a certain methodological problem because the data on electric and magnetic potentials in EEG and MEG are obtained using electrodes on the scalp. One needs to reconstruct the 3-dimensional distribution of electric and magnetic activity in the brain from the scalp data. In addition, fMRI

provides a single activity level per voxel in the statistical map, while EEG and MEG present in each voxel a time course of brain activity. Consequently, to obtain a single value per voxel, we had to take samples of the time course in EEG and MEG data and then compare these values with the fMRI spatial maps. These have inevitable limitations due to the different constraints of the techniques, which are compared in the study: the coarse-graining of time by fMRI/BOLD and the coarse-graining of space by EEG and MEG [42].

Contrast with the baseline for the images with gradients of activity is important because such differences exist even at rest due to the physiological differences in the metabolism levels between the white matter and the cortex. Thus, the task-specific analysis should include contrast with the baseline activity (scrambled faces in the data analysed here).

One should distinguish the source analysis in EEG and MEG from the spatial sources (divergences) in this study. The source analysis of EEG and MEG seeks out the sources in the brain that create the distribution of electric and magnetic energy on the scalp. Thus, its aim is to pass from the scalp to the space within the brain. Our analysis of spatial sources (divergences) is completely within the space of the brain and indicates brain clusters where the net flow of metabolic, electric, or magnetic energy from the particular voxels is outside (i.e., to the neighboring voxels).

Our approach does not use the temporal dimension because we consider the average brain activity for the given stimulation. In some previous studies, the optical flow equation, which includes gradients, was applied to the M/EEG data [43]. Although the computational base has similar features, optical flow analysis includes the temporal dimension and is not applicable to the temporally smoothed and averaged fMRI data. Thus, we do not compute activity flows *per se,* but rather the stable spatial directions of the flows (i.e., the directions along the paths at their loci of cortical input).

To find the optimal methodological pipeline, we used the existing datasets, which are very rare for multimodal stimulation with exactly the same stimuli. The statistical group analysis for specific stimulation would be the further application of this pipeline and will require a separate, specially designed study.

CONCLUSIONS

Our study provides further support that computation of brain activity gradients is a solid method that can be applied to different neuroimaging studies. In addition to studies of normal brain activity, this method of spatial differentiation can be used to clarify the topographies of brain activity in various diseases where the brain metabolism is estimated in 3-dimensional space using neuroimaging techniques. For example, a particularly interesting application of this method could be the localisation of activity sources in epilepsy [44]. The existing neuroimaging methods localize only the areas of increased activity in epilepsy; sources of this activity are thought to be somewhere inside or nearby, with their precise location remaining unclear (see [45] for discussion). In brain lesions, the present analysis may help estimate the compensatory reorganisation of brain function by demonstrating the directions of such reorganisation as well as the new sources from which the brain activity propagates. Thus, the proposed analysis of gradients and their sources in the brain could be widely used in medical research.

Conflict of Interest

There is no conflict of interest.

Acknowledgments: We thank R. Henson for the acquisition of the fMRI-EEG-MEG dataset, A. Babajani-Feremi for the acquisition of the MEG-fMRI dataset, and R. Vanrullen, R. Sokoliuk, N. Vayssiere and the staff of the Baudot technical platform for the simultaneous fMRI-EEG dataset. This work was supported by the DRCI Toulouse (Direction de la Recherche Clinique et de l'Innovation to Kuzma Strelnikov), the Midi-Pyrénnées region (RTT N 10006537 to Kuzma Strelnikov and Pascal Barone) and the recurrent funding of the CNRS (to Pascal Barone).

References and Notes

1. K. Friston, P. Fletcher, O. Josephs, A. Holmes, M. D. Rugg, and R. Turner, Event-related fMRI: Characterizing differential responses. *Neuroimage* 7, 30 **(1998)**.
2. C. D. Aizenman, A. Kirkwood, and M. F. Bear, A current source density analysis of evoked responses in slices of adult rat visual cortex: Implications for the regulation of long-term potentiation. *Cereb. Cortex* 6, 751 **(1996)**.
3. U. Mitzdorf, Current source-density method and application in cat cerebral cortex: Investigation of evoked potentials and EEG phenomena. *Physiol. Rev.* 65, 37 **(1985)**.
4. K. Strelnikov and P. Barone, Stable modality-specific activity flows as reflected by the neuroenergetic approach to the FMRI weighted maps. *PLoS One* 7, e33462 **(2012)**.
5. A. Kepecs, X. J. Wang, and J. Lisman, Bursting neurons signal input slope. *J. Neurosci.* 22, 9053 **(2002)**.
6. G. La Camera, M. Giugliano, W. Senn, and S. Fusi, The response of cortical neurons to *in vivo*-like input current: Theory and experiment: I. Noisy inputs with stationary statistics. *Biol. Cybern.* 99, 279 **(2008)**.
7. R. G. Shulman, D. L. Rothman, K. L. Behar, and F. Hyder, Energetic basis of brain activity: Implications for neuroimaging. *Trends Neurosci.* 27, 489 **(2004)**.
8. A. B. Patel, R. A. de Graaf, G. F. Mason, D. L. Rothman, R. G. Shulman, and K. L. Behar, The contribution of GABA to glutamate/glutamine cycling and energy metabolism in the rat cortex *in vivo*. *Proc. Natl. Acad. Sci. USA* 102, 5588 **(2005)**.
9. N. T. Markov, P. Misery, A. Falchier, C. Lamy, J. Vezoli, R. Quilodran, M. A. Gariel, P. Giroud, M. Ercsey-Ravasz, L. J. Pilaz, C. Huissoud, P. Barone, C. Dehay, Z. Toroczkai, D. C. Van Essen, H. Kennedy, and K. Knoblauch, Weight consistency specifies regularities of macaque cortical networks. *Cereb. Cortex* 21, 1254 **(2011)**.

RESEARCH ARTICLE

10. B. P. Rogers, V. L. Morgan, A. T. Newton, and J. C. Gore, Assessing functional connectivity in the human brain by fMRI. *Magn. Reson. Imaging* 25, 1347 **(2007)**.

11. B. J. Jellison, A. S. Field, J. Medow, M. Lazar, M. S. Salamat, and A. L. Alexander, Diffusion tensor imaging of cerebral white matter: A pictorial review of physics, fiber tract anatomy, and tumor imaging patterns. *AJNR Am. J. Neuroradiol.* 25, 356 **(2004)**.

12. K.-H. Cho, L.-W. Kuo, and C.-P. Lin, Mapping Brain connectomics from brownian motion: A technical review for diffusion MRI. *J. Neurosci. Neuroeng.* 2, 104 **(2013)**.

13. N. K. Logothetis, J. Pauls, M. Augath, T. Trinath, and A. Oeltermann, Neurophysiological investigation of the basis of the fMRI signal. *Nature* 412, 150 **(2001)**.

14. T. Kirschstein and R. Kohling, What is the Source of the EEG? *Clin. EEG Neurosci.* 40, 146 **(2009)**.

15. H. Stefan, N. Nakasato, and A. C. Papanicolaou, *Magnetoencephalography. Handb. Clin. Neurol.* 107, 347 **(2012)**.

16. V. E. Griffeth, N. P. Blockley, A. B. Simon, and R. B. Buxton, A new functional MRI approach for investigating modulations of brain oxygen metabolism. *PLoS One* 8, e68122 **(2013)**.

17. C. W. Wu and Y.-P. Chao, Fundamental concerns for detecting synchronized brain networks using resting-state functional magnetic resonance imaging. *J. Neurosci. Neuroeng.* 1, 193 **(2012)**.

18. Z. Liu, C. Rios, N. Zhang, L. Yang, W. Chen, and B. He, Linear and nonlinear relationships between visual stimuli, EEG and BOLD fMRI signals. *Neuroimage* 50, 1054 **(2010)**.

19. A. G. Goloshevsky, A. C. Silva, S. J. Dodd, and A. P. Koretsky, BOLD fMRI and somatosensory evoked potentials are well correlated over a broad range of frequency content of somatosensory stimulation of the rat forepaw. *Brain Res.* 1195, 67 **(2008)**.

20. G. Rees, K. Friston, and C. Koch, A direct quantitative relationship between the functional properties of human and macaque V5. *Nat. Neurosci.* 3, 716 **(2000)**.

21. D. J. Heeger, A. C. Huk, W. S. Geisler, and D. G. Albrecht, Spikes versus BOLD: What does neuroimaging tell us about neuronal activity? *Nat. Neurosci.* 3, 631 **(2000)**.

22. A. Ekstrom, How and when the fMRI BOLD signal relates to underlying neural activity: The danger in dissociation. *Brain Res. Rev.* 62, 233 **(2010)**.

23. R. N. Henson, J. Mattout, K. D. Singh, G. R. Barnes, A. Hillebrand, and K. Friston, Population-level inferences for distributed MEG source localization under multiple constraints: Application to face-evoked fields. *Neuroimage* 38, 422 **(2007)**.

24. R. N. Henson, J. Mattout, C. Phillips, and K. J. Friston, Selecting forward models for MEG source-reconstruction using model-evidence. *Neuroimage* 46, 168 **(2009)**.

25. R. N. Henson, E. Mouchlianitis, and K. J. Friston, MEG and EEG data fusion: Simultaneous localisation of face-evoked responses. *Neuroimage* 47, 581 **(2009)**.

26. S. J. Kiebel and K. J. Friston, Statistical parametric mapping for event-related potentials (II): A hierarchical temporal model. *Neuroimage* 22, 503 **(2004)**.

27. R. N. Henson, T. Shallice, M. L. Gorno-Tempini, and R. J. Dolan, Face repetition effects in implicit and explicit memory tests as measured by fMRI. *Cereb Cortex* 12, 178 **(2002)**.

28. A. Babajani-Feremi, H. Soltanian-Zadeh, and J. E. Moran, Integrated MEG/fMRI model validated using real auditory data. *Brain Topogr.* 21, 61 **(2008)**.

29. H. Laufs, J. Daunizeau, D. W. Carmichael, and A. Kleinschmidt, Recent advances in recording electrophysiological data simultaneously with magnetic resonance imaging. *Neuroimage* 40, 515 **(2008)**.

30. S. Debener and M. De Vos, The benefits of simultaneous EEG-fMRI for EEG analysis. *Clin. Neurophysiol.* 122, 217 **(2011)**.

31. R. K. Niazy, C. F. Beckmann, G. D. Iannetti, J. M. Brady, and S. M. Smith, Removal of FMRI environment artifacts from EEG data using optimal basis sets. *Neuroimage* 28, 720 **(2005)**.

32. K. Friston, L. Harrison, J. Daunizeau, S. Kiebel, C. Phillips, N. Trujillo-Barreto, R. Henson, G. Flandin, and J. Mattout, Multiple sparse priors for the M/EEG inverse problem. *Neuroimage* 39, 1104 **(2008)**.

33. R. C. Sotero and N. J. Trujillo-Barreto, Biophysical model for integrating neuronal activity, EEG, fMRI and metabolism. *Neuroimage* 39, 290 **(2008)**.

34. K. Strelnikov, Neuroimaging and neuroenergetics: Brain activations as information-driven reorganization of energy flows. *Brain Cogn.* 72, 449 **(2010)**.

35. A. Mayevsky, J. Sonn, and E. Barbiro-Michaely, Physiological mapping of brain functions *in vivo*: Surface monitoring of hemodynamic metabolic ionic and electrical activities in real-time. *J. Neurosci. Neuroeng.* 2, 150 **(2013)**.

36. FIL, SPM8: http://www.fil.ion.ucl.ac.uk/spm/software/spm8/ **(2012)**.

37. J. Carpenter and J. Bithell, Bootstrap confidence intervals: When, which, what? A practical guide for medical statisticians. *Stat. Med.* 19, 1141 **(2000)**.

38. J. Daunizeau, H. Laufs, and K. Friston, EEG-fMRI information fusion: Biophysics and data analysis, EEG-fMRI-Physiology, Technique and Applications, edited by C. Mulert and L. Lemieux, Springer DE, Berlin **(2010)**.

39. P. A. Valdes-Sosa, J. M. Sanchez-Bornot, R. C. Sotero, Y. Iturria-Medina, Y. Aleman-Gomez, J. Bosch-Bayard, F. Carbonell, and T. Ozaki, Model driven EEG/fMRI fusion of brain oscillations. *Hum. Brain Mapp.* 30, 2701 **(2009)**.

40. O. David and K. J. Friston, A neural mass model for MEG/EEG: coupling and neuronal dynamics. *Neuroimage* 20, 1743 **(2003)**.

41. R. Srinivasan, W. R. Winter, and P. L. Nunez, Source analysis of EEG oscillations using high-resolution EEG and MEG. *Prog. Brain Res.* 159, 29 **(2006)**.

42. W. J. Freeman, S. P. Ahlfors, and V. Menon, Combining fMRI with EEG and MEG in order to relate patterns of brain activity to cognition. *Int. J. Psychophysiol.* 73, 43 **(2009)**.

43. J. Lefevre and S. Baillet, Optical flow approaches to the identification of brain dynamics. *Hum. Brain Mapp.* 30, 1887 **(2009)**.

44. H. Stefan and F. H. Lopes da Silva, Epileptic neuronal networks: Methods of identification and clinical relevance. *Front. Neurol.* 4, 8 **(2013)**.

45. D. N. Lenkov, A. B. Volnova, A. R. Pope, and V. Tsytsarev, Advantages and limitations of brain imaging methods in the research of absence epilepsy in humans and animal models. *J. Neurosci. Methods* 212, 195 **(2013)**.

RESEARCH ARTICLE